

Kinetic and Structural Studies on the Interaction of Cholinesterases with the Anti-Alzheimer Drug Rivastigmine^{†,‡}

P. Bar-On,^{§,||} C. B. Millard,^{§,⊥} M. Harel,^{||} H. Dvir,^{§,||} A. Enz,[@] J. L. Sussman,^{||} and I. Silman^{*,§}

Departments of Neurobiology and Structural Biology, Weizmann Institute of Science, Rehovot 76100, Israel, and Preclinical Research (CNS), Novartis Pharma AG, Basel CH4002, Switzerland

Received January 8, 2002

ABSTRACT: Rivastigmine, a carbamate inhibitor of acetylcholinesterase, is already in use for treatment of Alzheimer's disease under the trade name of Exelon. Rivastigmine carbamylates *Torpedo californica* acetylcholinesterase very slowly ($k_i = 2.0 \text{ M}^{-1} \text{ min}^{-1}$), whereas the bimolecular rate constant for inhibition of human acetylcholinesterase is >1600-fold higher ($k_i = 3300 \text{ M}^{-1} \text{ min}^{-1}$). For human butyrylcholinesterase and for *Drosophila melanogaster* acetylcholinesterase, carbamylation is even more rapid ($k_i = 9 \times 10^4$ and $5 \times 10^5 \text{ M}^{-1} \text{ min}^{-1}$, respectively). Spontaneous reactivation of all four conjugates is very slow, with <10% reactivation being observed for the *Torpedo* enzyme after 48 h. The crystal structure of the conjugate of rivastigmine with *Torpedo* acetylcholinesterase was determined to 2.2 Å resolution. It revealed that the carbamyl moiety is covalently linked to the active-site serine, with the leaving group, (–)-S-3-[1-(dimethylamino)ethyl]phenol, being retained in the “anionic” site. A significant movement of the active-site histidine (H440) away from its normal hydrogen-bonded partner, E327, was observed, resulting in disruption of the catalytic triad. This movement may provide an explanation for the unusually slow kinetics of reactivation.

The principal role of acetylcholinesterase (AChE)¹ is termination of impulse transmission at cholinergic synapses by rapid hydrolysis of acetylcholine (ACh) (1). In keeping with this requirement, AChE possesses a remarkably high specific activity for a serine hydrolase, displaying a turnover number of $\sim 10000 \text{ s}^{-1}$, and thus operating close to the diffusion-controlled limit (2). Determination of the three-dimensional (3D) structure of *Torpedo californica* AChE (TcAChE) revealed that AChE contains a catalytic triad similar to that present in other serine hydrolases. Unexpectedly, it also revealed that this triad is located near the bottom

of a deep and narrow gorge, ca. 20 Å in depth, named the “aromatic gorge” (3).

Reduction of cortical and CSF cholinergic markers, such as AChE and choline acetyl transferase and ACh itself, is correlated both with the extent of the neuropathology and with the severity of cognitive impairment in Alzheimer's disease (AD) (4, 5). This led to the hypothesis that AD is associated with cholinergic insufficiency (6–8). This serves as the rationale for the use of AChE inhibitors (AChEIs) for the symptomatic treatment of AD in its early stages to elevate the levels of ACh in the brain, and thus to ameliorate cognitive deficits (9).

The only approach approved so far for the treatment of AD is the use of AChEIs. Three types of AChEI have been employed: (1) classical reversible inhibitors, which are generally tertiary amines; (2) irreversible inhibitors, such as organophosphates (OPs), that covalently phosphorylate or phosphonylate the esteratic site of the enzyme; and (3) slow substrates, typified by the carbamates, that also react covalently with the enzyme (9). The drugs approved so far include natural substances, such as huperzine A (10), and galanthamine under its trade name Reminyl (11, 12), and synthetic compounds, such as tacrine under its trade name Cognex (13, 14) and E2020 under its trade name Aricept (15, 16).

The alkaloid, physostigmine, was shown to display cholinergic activity, and it was subsequently demonstrated that this was due to its anticholinesterase activity (17). Elucidation of the chemical structure of physostigmine (18) was followed by rapid progress in the development of synthetic AChEIs, which was pioneered by Stedman and co-workers (19). The first synthetic carbamate to find clinical application was

[†] This study was supported by the Kimmelman Center for Molecular Structure and Assembly and the Benozio Center for Neurosciences. C.B.M. was supported by the U.S. Army Scientist/Engineer Exchange Program.

[‡] Coordinates and structure factors for the TcAChE–rivastigmine conjugate and the TcAChE–NAP complex have been deposited in the Protein Data Bank, as entries 1gqr and 1gqs, respectively.

^{*} To whom correspondence should be addressed. Fax: +972-8-947-1849.

[§] Department of Neurobiology.

^{||} Department of Structural Biology.

[⊥] Present address: U.S. Army Medical Research Institute of Infectious Diseases, 1425 Porter St., Fort Detrick, MD 21702-5011.

[@] Novartis Pharma.

¹ Abbreviations: ACh, acetylcholine; AChE, acetylcholinesterase; AD, Alzheimer's disease; ANS, 1-anilino-8-naphthalenesulfonic acid; ATCh, acetylthiocholine; BChE, butyrylcholinesterase; BSA, bovine serum albumin; BTCh, butyrylthiocholine; ChE, cholinesterase; *Dm*, *Drosophila melanogaster*; DTNB, 5,5'-dithiobis(2-nitrobenzoic acid); EMCC, *N,N*-ethylmethylcarbamyl chloride; h, human; NAP, (–)-S-3-[1-(dimethylamino)ethyl]phenol; PEG, polyethylene glycol; PMSF, phenylmethanesulfonyl fluoride; r, recombinant; *Tc*, *Torpedo californica*; TMB-4, 1,1'-(1,3-propanediyl)bis[4-(hydroxyimino)methyl]pyridinium dibromide; VX, *O*-ethyl-S-[2-[bis(1-methylethyl)amino]ethyl]-methylphosphonothioate; 2-PAM, pyridine-2-aldoxime methiodide; 3D, three-dimensional; 3-PAM, pyridine-3-aldoxime methiodide.

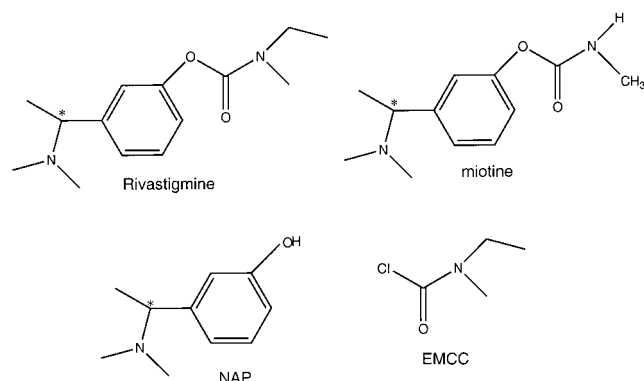


FIGURE 1: AChE inhibitors.

appropriately named miotine (Figure 1), due to its miotic activity (20, 21), and the Stedman laboratory carried out extensive pharmacological studies on miotine and its analogues (22, 23). Weinstock and co-workers (24, 25) synthesized a series of analogues of miotine in which the chain length and branching of the alkyl substituents on the carbamyl moiety were varied. Several of these compounds were less toxic, in particular disubstituted derivatives, and had a longer duration of action than physostigmine, which, at that time, had already been tested as a potential anti-Alzheimer drug (26). The (–)-stereoisomer of the *N,N*-methyleneethylcarbamyl derivative, rivastigmine {(–)-*S*-ethyl-3-[1-(dimethylamino)ethyl]-*N*-methylphenylcarbamate hydrogen tartrate, SDZ ENA-713, Figure 1}, was selected for clinical trials, due to its 10-fold greater affinity for brain G_1 AChE over peripheral forms of the enzyme, its chemical stability, its longer duration of action in vivo, and its good tolerability (27). It was approved by the European Agency for the Evaluation of Medicinal Products in 1998, and by the FDA in 2000, under the trade name of Exelon, for the treatment of AD.

In this study, we first characterized the kinetics of the interaction of rivastigmine with various types of AChE and with human butyrylcholinesterase (hBChE). To understand the structural basis for the observed kinetic phenomena, the 3D structures of the conjugate of rivastigmine and the complex of its leaving group (–)-*S*-3-[1-(dimethylamino)ethyl]phenol (NAP, Figure 1) with *Tc*AChE were determined by X-ray crystallography.

MATERIALS AND METHODS

Enzymes. The dimeric form of *Tc*AChE was purified from electric organ tissue of *T. californica* by affinity chromatography after solubilization with phosphatidylinositol-specific phospholipase C (28–30). The enzyme was stored in 100 mM NaCl, 0.02% sodium azide, and 1 mM 2-(*N*-morpholino)ethanesulfonic acid (MES) at pH 6.5 and 4 °C. Serum hBChE (31) was a gift from Y. Ashani (Israel Institute for Biological Research, Ness Ziona, Israel). Recombinant human AChE (rhAChE) (32) and recombinant *Drosophila melanogaster* (*rDm*AChE) (33) were gifts from T. L. Rosenberry (Mayo Clinic, Jacksonville, FL).

ChE Inhibitors. Rivastigmine, its optical isomer SDZ 212-712, *N,N*-ethylmethylcarbamyl chloride (EMCC, Figure 1), and NAP were from Novartis Pharma AG. Rivastigmine, SDZ 212-712, and NAP were dissolved in water. EMCC was dissolved in acetonitrile.

Reactivators. Hydroxylamine, pyridine-2-aldoxime methiodide (2-PAM), pyridine-3-aldoxime methiodide (3-PAM), and 1,1'-(1,3-propanediyl)bis[4-(hydroxyimino)methyl]pyridinium dibromide (TMB-4) were obtained from the U.S. Army Medical Research Institute of Chemical Defense (Aberdeen, MD).

Others. Acetylthiocholine (ATCh), 1-anilino-8-naphthalenesulfonic acid (ANS), bovine serum albumin (BSA), butyrylthiocholine (BTCh), 5,5'-dithiobis(2-nitrobenzoic acid) (DTNB), Bio-Gel P-6, 2-(*N*-morpholino)ethanesulfonic acid (MES), and polyethylene glycol 200 (PEG 200) were all purchased from Sigma Chemicals (St. Louis, MO). Bio-spin disposable chromatography columns were from Bio-Rad Laboratories (Hercules, CA). Acetonitrile for HPLC was purchased from Bio-Lab Ltd. (Jerusalem, Israel).

Enzymic Activity. Enzymic activity was determined by the Ellman procedure (34) using ATCh as a substrate for AChE, and BTCh for hBChE. The reaction was monitored by following the change in absorbance (ΔAU) spectrophotometrically, at 412 nm, in a Uvikon 940 spectrophotometer. The standard assay was carried out as follows. Appropriate enzyme aliquots were added to a cuvette containing 1 mL of assay mixture (1 mM ATCh or BTCh, 0.3 mM DTNB, and 0.01% BSA) in 0.067 M Na/K phosphate (pH 7.5). The reaction was monitored for 1 min. Measurements were performed at 25 °C unless otherwise stated.

Inhibition Constants. The inhibition constant (K_i) for inhibition of *Tc*AChE by NAP was determined using several different substrate and inhibitor concentrations. K_i was determined using a program that first calculated K_m and V_{max} at each inhibitor concentration. The value of K_i was then obtained from the intersection of the linear plot of K_m/V_{max} versus [NAP] with the x -axis, as described by Cornish-Bowden (35).

Bimolecular Rate Constant for Carbamylation. The apparent bimolecular rate constants (k_i) were determined from the pseudo-first-order rate constants (k_{obs}) for progressive inhibition at several inhibitor concentrations.

Spontaneous Reactivation. Enzyme was inhibited $\geq 95\%$. Excess inhibitor was removed either by dilution into 0.067 M Na/K phosphate (pH 7.5), by dialysis into that buffer, or by gel filtration under centrifugal force (36), using columns packed with Bio-Gel P-6 that had been pre-equilibrated with 0.067 M Na/K phosphate (pH 7.5). Column eluates (enzyme) were placed immediately in a water bath to control the temperature. Samples were withdrawn at successive time points, and assayed to measure recovery of enzyme activity. The percentage of reactivation was determined by comparison of enzymic activity with that for control column eluates, where the enzyme had been mixed with buffer instead of inhibitor, but otherwise treated identically. The apparent decarbamylation rate constant (k_3) was determined from the fit of the exponential data points to a single exponential.

Spectroscopic Measurements. The intrinsic fluorescence of AChE samples was measured in a Shimadzu RF-540 spectrofluorometer, with excitation at 295 nm, and emission measured at 300–400 nm. Binding of ANS was assessed as follows. Aliquots (2 μ L) of 0.1 mM ANS in acetonitrile were added to 200 μ L of 0.5 μ M *Tc*AChE in 0.067 M Na/K phosphate (pH 7.5). Excitation was at 390 nm, and emission was measured between 400 and 600 nm, employing a Shimadzu RF-540 spectrofluorometer at room temperature.

Table 1: Data Collection and Processing Statistics

	rivastigmine	NAP
space group	<i>P</i> 3(1)21	<i>P</i> 3(1)21
no. of monomers in ASU	1	1
cell axes (Å)	112.052, 112.052, 136.77	111.040, 111.040, 137.227
cell angles (deg)	90, 90, 120	90, 90, 120
wavelength (Å)	1.10	1.54
temperature (K)	100	100
diffraction limit (Å)	2.2	3.0
no. of measured reflections	242981	243327
no. of unique reflections	50861	20244
no. of unique reflections used	46214	20097
completeness (%)	99.7 ^a (97.1) ^b	99.4 ^a (98.4) ^b
<i>R</i> _{sym} (on <i>I</i>) (%)	6.6 ^a (32.2) ^b	16.0 ^a (52.9) ^b
<i>I</i> / σ (<i>I</i>)	17.7 ^a (1.4) ^b	5.0 ^a (1.4) ^b

^a All data. ^b Highest-resolution range of 2.28–2.20 Å for rivastigmine and 3.11–3.00 Å for NAP.

Circular dichroism (CD) measurements were performed in a Jasco J500C spectropolarimeter, using 0.2 mm and 1 cm path length cuvettes for near- and far-UV measurements, respectively. Azide-free samples of enzyme (0.5 mg/mL) in 0.067 M Na/K phosphate (pH 7.5) were employed.

X-ray Crystallography. Trigonal crystals of native *TcAChE* were obtained by the hanging-drop vapor-diffusion method, using as a precipitant 34–38% (v/v) PEG 200 in 0.1 M MES at pH 5.8 and 4 °C, and a protein concentration of 11 mg/mL (30). The drops contained 2 μ L of a protein solution and 2 μ L of a precipitant solution. The *TcAChE*–rivastigmine conjugate and the *TcAChE*–NAP complex were obtained by soaking the native crystals for 13 days in mother liquor containing 3 mM rivastigmine or for 5 days in mother liquor containing 2 mM NAP. Crystals were immersed briefly in high-viscosity motor oil (Exxon, Houston, TX), and flash-frozen in liquid nitrogen prior to data collection at 100 K. For the rivastigmine conjugate, data were collected to 2.2 Å resolution on beam line X12C of the U.S. National Synchrotron Light Source at Brookhaven National Laboratory (Upton, NY). For the NAP complex, data were collected to 3.0 Å resolution “in house” at the Weizmann Institute of Science, using a Rigaku R-AXIS-IIC imaging plate detector mounted on a Rigaku FR rotating anode. Data collection and statistics parameters for the two structures are summarized in Table 1.

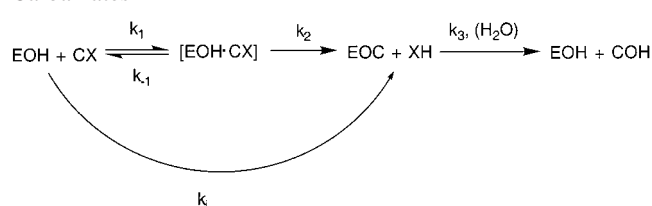
The structures were determined by molecular replacement using the 2.5 Å structure of native *TcAChE* [Protein Data Bank (PDB) entry 2ACE (30)] as a starting model, with no solvent molecules or attached sugars. The structures were refined by a combination of simulated annealing and molecular dynamics with a maximum likelihood target function, using the CNS program suite (37, 38). Refinement and model statistics results for both structures are summarized in Table 2.

RESULTS

Carbamylation of *TcAChE* by Rivastigmine. Earlier kinetic studies, performed on human erythrocyte AChE, treated rivastigmine as a slow-binding reversible inhibitor, with an apparent *K*_i of \sim 200 μ M (25). Although such an approach provides a useful, subjective comparison of inhibitor potency for a particular set of conditions, it is formally incomplete.

Table 2: Refinement Data and Model Statistics

	rivastigmine	NAP
resolution range (Å)	29.2–2.2	29.2–3.0
no. of reflections	46026	20004
<i>R</i> -factor (%)		
work	19.9	21.2
free	23.6	26.2
no. of atoms		
protein (535 residues)	4193	4245
hetero (carbohydrate, solvent, inhibitor)	440	245
average <i>B</i> -factor		
protein	32.9	41.7
water	51.2	31.0
carbohydrate	46.5	69.8
rmsd from ideal values		
bond lengths (Å)	0.006	0.008
bond angles (deg)	1.3	1.4
dihedral angles (deg)	23.7	23.0
improper torsion angles (deg)	1.13	0.90
estimated coordinate error		
low-resolution cutoff (Å)	5.0	5.0
ESD from Luzzati plot (Å)	0.30	0.36
ESD from SigmaA (Å)	0.32	0.66

Scheme 1: Mechanism of Inhibition of ChEs by Carbamates^a

^a The carbamate forms a complex with AChE prior to carbamylation, and decarbamylation proceeds through attack of water (under conditions where $k_3 \ll k_2$). EOH, enzyme; CX, intact carbamate; k_1 , rate constant for the formation of the reversible complex [EOH·CX]; k_{-1} , rate constant for dissociation of the [EOH·CX] complex; k_2 , carbamylation rate constant; EOC, carbamylated enzyme; XH, leaving group; k_3 , decarbamylation rate constant; COH, hydrolyzed carbamate, a carbamic acid derivative; k_i , apparent bimolecular rate constant governing the overall rate of inhibition and neglecting the formation of the reversible complex.

Wilson and co-workers demonstrated that carbamates serve as slow substrates of AChE (Scheme 1), with rapid carbamylation being followed by much slower decarbamylation (39, 40).

Covalent reaction between *TcAChE* and rivastigmine was suggested by the progressive inhibition of *TcAChE* by rivastigmine (Figure 2, left). Inhibition was relatively slow, requiring millimolar concentrations of inhibitor to significantly reduce enzyme activity. The apparent k_i for carbamylation was 2.0 $M^{-1} \text{ min}^{-1}$ (Figure 2, right).

Decarbamylation of *TcAChE* Inhibited by Rivastigmine. To determine if rivastigmine behaves as a slow substrate of *TcAChE*, spontaneous decarbamylation studies were carried out. Unexpectedly, the inhibition of *TcAChE* by rivastigmine displayed very slow reactivation (<10% after 48 h) using the gel filtration method of reactivation. We attempted, therefore, to accelerate the reactivation of the carbamylated enzyme by several means. The addition of nucleophiles, after gel filtration, including hydroxylamine, and the oximes 2-PAM, 3-PAM, and TMB-4, had no significant effect on the apparent rate of reactivation. Moreover, neither extensive washing on Amicon filters nor dialysis of the inhibited

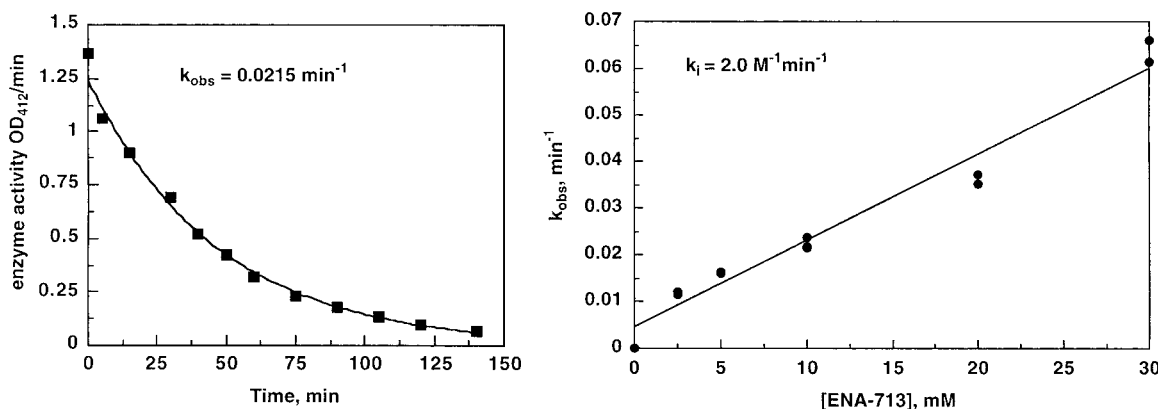


FIGURE 2: Overall carbamylation of *TcAChE* with rivastigmine. Pseudo-first-order inhibition rates (k_{obs}) were determined by measuring the residual activity of *TcAChE* as a function of time in the presence of rivastigmine (2.5–30 mM). The left panel shows a representative determination of k_{obs} at a single inhibitor concentration (10 mM). The points are experimental data, and the curve is a direct fit to a single-exponential decay. The right panel shows a linear relationship between pseudo-first-order rate constants and rivastigmine concentrations. The slope of this line is the apparent bimolecular rate constant.

enzyme for 24 h at 4 °C resulted in faster or greater reactivation of the carbamylated *TcAChE*.

The fact that decarbamylation was slow compared to that of carbamyl-AChE conjugates produced by other carbamates (41) raised the possibility that inhibition by rivastigmine might induce a conformational change in the enzyme. Accordingly, spectroscopic experiments were performed to check whether inhibition by rivastigmine caused (1) exposure of hydrophobic surfaces; (2) a red shift in the emission peak for intrinsic fluorescence, which would indicate that the indole rings of tryptophan residues are more exposed to the solvent than in the native form of the enzyme; and (3) a change in ellipticity. No evidence for a substantial conformational change upon carbamylation with rivastigmine was observed by these methods, suggesting that the enzyme was neither fully denatured nor in one of the previously described catalytically inactive molten globule or quasi-native states (42).

Reversible Inhibition of *TcAChE* by NAP. The leaving group of rivastigmine (XH in Scheme 1), NAP, is a phenol ring bearing a tertiary nitrogen substituent. It has a structure similar to that of edrophonium, a well-studied competitive inhibitor of AChE (13). Figure 3 shows that NAP is a competitive reversible inhibitor of *TcAChE* with a K_i of 0.5 μM . This raised the possibility that the product of carbamylation might influence the interaction of *TcAChE* and rivastigmine.

Kinetics of Inhibition of *TcAChE* by EMCC. To isolate the contribution of the NAP moiety to the kinetics of inhibition and reactivation of *TcAChE* by rivastigmine, we studied the kinetics of the reaction of *TcAChE* with the homologous carbamate, EMCC, in which chloride replaces NAP as the leaving group. EMCC inhibited *TcAChE* substantially faster than rivastigmine, displaying a k_i value of 20 $\text{M}^{-1} \text{ min}^{-1}$. Upon dilution, complete reactivation was observed, with a decarbamylation rate constant of 0.03 min^{-1} , and a $t_{1/2}$ of 25 min (Figure 4). Addition of 2 μM NAP to the reaction mixture after dilution had no effect on the rate or extent of reactivation (Figure 4), and similar results were obtained when NAP was added before dilution (data not shown). Thus, failure of the *TcAChE*–rivastigmine conjugate to reactivate cannot simply be ascribed to stabilization of the ethylmethylcarbamylated *TcAChE* by NAP.

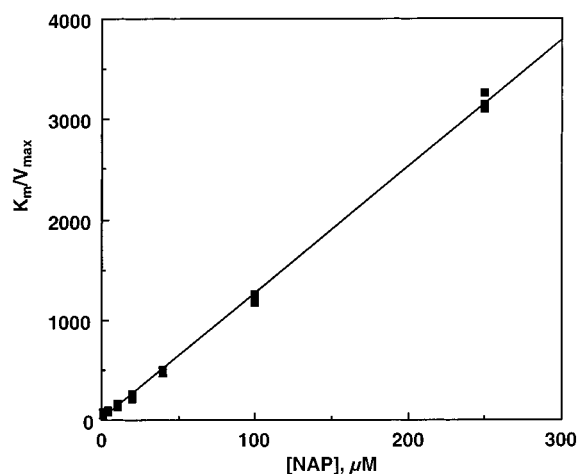


FIGURE 3: Reversible inhibition of *TcAChE* by NAP. The inhibition constant for reversible inhibition of *TcAChE* with NAP was measured using the method of a K_m/V_{max} plot (35) at seven different concentrations of NAP in the range of 0.15–1 mM. The results show that NAP is a competitive inhibitor of *TcAChE*.

Kinetic Characterization of the Action of Rivastigmine on *rhAChE*, *rDmAChE*, and *hBChE*. The kinetic results for the inactivation of *TcAChE* by rivastigmine were unexpected. To determine whether both the observed slow inhibition of *TcAChE* by rivastigmine and the extremely slow reactivation were species-specific, we extended our kinetic studies to other ChEs. *rhAChE* seemed particularly relevant since it is the *in vivo* target of rivastigmine as an AD drug. We also studied *hBChE*, and *rDmAChE*, the 3D structure of which was recently determined (43).

Rivastigmine inhibited *rhAChE* very much faster than *TcAChE* at 25 °C. The bimolecular rate for inhibition of *rhAChE* was more than 1600-fold higher than for *TcAChE* (3300 vs 2.0 $\text{M}^{-1} \text{ min}^{-1}$, respectively), requiring a micromolar instead of a millimolar inhibitor concentration to reduce enzyme activity significantly. However, for *rhAChE*, too, no reactivation could be detected by the dialysis method, and only 25% reactivation was observed after 48 h at 25 °C using the gel filtration method (Table 3). Whereas *TcAChE* is relatively heat-sensitive (44), the thermal stability of *rhAChE* permitted us to perform experiments at the physiological temperature (37 °C). The bimolecular rate constant

Table 3: Kinetic Constants for the Interaction of ChEs with Rivastigmine and SDZ 212-712^a

enzyme	rivastigmine		SDZ 212-712	
	k_i ($M^{-1} \text{ min}^{-1}$)	% reactivation	k_i ($M^{-1} \text{ min}^{-1}$)	% reactivation
<i>TcAChE</i>	2.0 ± 0.05	<10	$\leq 0.3^b$	ND ^c
rhAChE	3300 ± 700	26 ± 3	110 ± 5	15–25
	5500 ± 500 (37 °C)	60 ± 1 (37 °C)	620 ± 50 (37 °C)	40–50 (37 °C)
<i>rDmAChE</i>	$(5 \pm 0.03) \times 10^5$	75 ± 4	$(11 \pm 0.1) \times 10^3$	40–50
hBChE	$(9 \pm 0.8) \times 10^4$	<10 (24 h) >80 (24 h, 37 °C)	ND ^c	ND ^c

^a Experiments were performed in 0.067 M Na/K phosphate at pH 7.5 and 25 °C, unless otherwise stated, as described in Materials and Methods. Reactivation was assessed for 48 h unless otherwise stated. The kinetic constants are expressed as the mean of at least three separate experiments. ^b Estimated value. ^c Not determined.

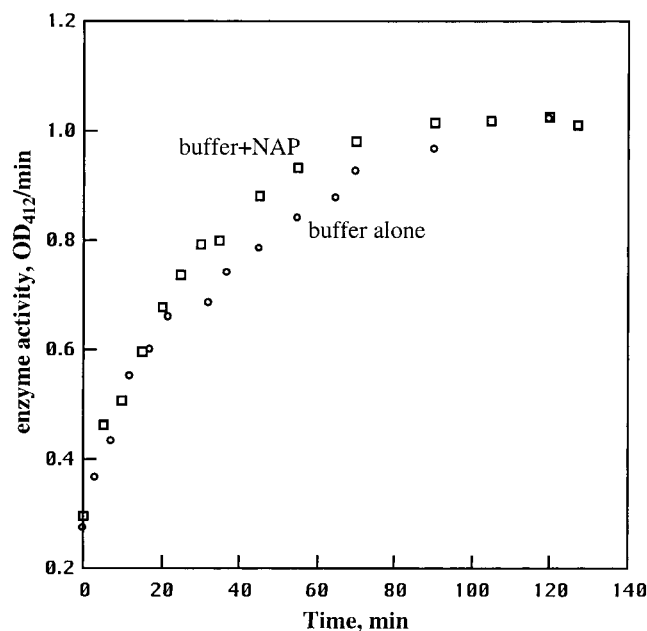


FIGURE 4: Decarbamylation of *TcAChE* inhibited by EMCC. *TcAChE* was inhibited >95% by employing 10 mM EMCC. Samples were then diluted 50-fold into buffer or into buffer containing 2 μ M NAP, and enzymic activity was determined as a function of time. Control samples of uninhibited *TcAChE* were otherwise treated identically.

Table 4: Kinetic Constants for NAP and EMCC Reacting with *TcAChE*, rhAChE, and hBChE^a

enzyme	NAP	EMCC	
	K_i (μ M)	k_i ($M^{-1} \text{ min}^{-1}$)	k_3 (min^{-1})
<i>TcAChE</i>	0.7 ± 0.4	20 ± 3	0.03 ± 0.0007
rhAChE	33 ± 2	unmeasurable	0.19 ± 0.003
hBChE	ND ^b	ND ^b	0.02 ± 0.002

^a Experiments were performed in 0.067 M Na/K phosphate at pH 7.5 and 25 °C, as described in Materials and Methods. The kinetic constants are expressed as the mean of three separate determinations. ^b Not determined.

for inhibition of rhAChE at 37 °C was $5500 M^{-1} \text{ min}^{-1}$, and 60% reactivation could be obtained within 48 h (Table 3). Carbamylation of rhAChE by EMCC was too fast to be assessed by the progressive inhibition method, and rapid hydrolysis of EMCC prevented attempts to follow the reaction at lower reagent concentrations. However, EMCC-inhibited rhAChE underwent complete spontaneous reactivation, with a $t_{1/2}$ of 4 min at 25 °C (Table 4).

The bimolecular rate constant for the carbamylation of hBChE by rivastigmine was almost 30-fold greater (9×10^4

$M^{-1} \text{ min}^{-1}$) than that of rhAChE (Table 3). As had been found with *TcAChE*, however, <10% reactivation of rivastigmine-inhibited hBChE was observed after 24 h at 25 °C. Again, the greater thermal stability of hBChE, relative to that of *TcAChE*, allowed us to perform reactivation experiments at a higher temperature. At 37 °C, reactivation of rivastigmine-inhibited hBChE was very slow, but went to >80% completion with a $t_{1/2}$ of approximately 24 h (Table 3). Moreover, complete and rapid reactivation of hBChE inhibited by EMCC was observed (Table 4).

The bimolecular rate constant for carbamylation of *rDmAChE* by rivastigmine at 25 °C was $5 \times 10^5 M^{-1} \text{ min}^{-1}$, and 75% reactivation was obtained within 48 h at the same temperature (Table 3).

Kinetic Characterization of SDZ 212-712. Rivastigmine was originally synthesized as a racemic mixture, but it was subsequently found that the (–)-*S*-isomer is the more potent compound, which was accordingly taken for development as an anti-AD drug. We compared the kinetic properties of rivastigmine and of its optical isomer, SDZ 212-712, and indeed found that the concentration of SDZ 212-712 we had to use, to reduce enzymic activity of rhAChE and of *rDmAChE* significantly, was 10-fold higher than that of rivastigmine. The bimolecular rate constant values for carbamylation of rhAChE and *rDmAChE* by SDZ 212-712 are thus much lower, 30- and 45-fold, respectively, compared to the k_i values for rivastigmine (Table 3). For *TcAChE* inhibited by SDZ 212-712, the k_i value could not be determined, since we could not reach a concentration of inhibitor that was sufficiently high to achieve significant inhibition. Reactivation of rhAChE and *rDmAChE* inhibited with SDZ 212-712 was also slower than that of the corresponding rivastigmine conjugates (Table 3).

3D Crystal Structure of the *TcAChE*–Rivastigmine Conjugate. The overall crystal structure of the *TcAChE*–rivastigmine conjugate is very similar to the native *TcAChE* structure (rmsd of 0.26 Å). The structure in the vicinity of the active site is shown in Figure 5. As might be expected, the highest positive-difference density peaks were observed at the bottom of the active-site gorge. One peak is seen at a position near S200, within covalent bonding distance of S200 O γ (1.39 Å), and another in proximity to both W84 and F330. Neither peak could account for the full rivastigmine molecule, but the carbamyl moiety of rivastigmine fitted the density abutting the active-site serine, S200, and the hydrolysis product, NAP, fitted the density at the other site, which corresponds to the “anionic” subsite of the active site (13, 45). The covalently bound carbamyl refined well, with full occupancy and a low temperature factor, suggesting a

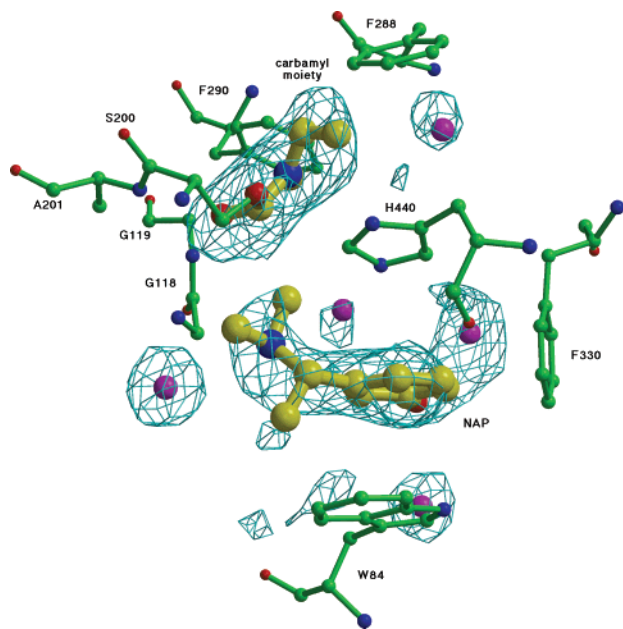


FIGURE 5: Electron density map of the *TcAChE*–rivastigmine conjugate. The map shows that both parts of rivastigmine, the carbamyl moiety and NAP, are retained in the active-site gorge, but detached from each other. Rivastigmine is rendered as a ball-and-stick model, with carbon atoms colored yellow, oxygen atoms colored red, and nitrogen atoms colored blue. Selected key protein residues in the vicinity of the conjugate are also rendered in ball-and-stick format, with carbon atoms colored green, and labeled appropriately.

stoichiometric (1:1) reaction between S200 and rivastigmine. The distance between the carbonyl carbon atom of the carbamyl moiety and the hydroxyl oxygen atom of NAP is 8.0 Å, thus supporting our conclusion that carbamylation had occurred, and that the NAP moiety had been detached from the carbamyl group (Figure 6). The refinement suggested only 80% occupancy by the NAP moiety. The carbamyl moiety is oriented with the carbonyl oxygen atom pointing into the oxyanion hole toward G119N and A201N (Figure 6), and the amino moiety toward F288 and F290 in the acyl pocket (Figure 6). The phenyl ring of the NAP moiety is stacked against the indole ring of W84 and oriented in herringbone fashion with respect to the phenyl ring of F330, thus interacting with the two aromatic residues implicated previously in quaternary ligand stabilization within the anionic site (13, 45). Its hydroxyl oxygen forms three H-bonds with three water molecules, two of which are among the conserved waters in the active site (46), and its amino nitrogen points toward the oxyanion hole, forming an H-bond with G118N.

Comparison of the native *TcAChE* structure with that of the *TcAChE*–rivastigmine conjugate reveals a substantial change in the position of the imidazole ring of the histidine residue in the catalytic triad, H440 (Figure 7). Thus, the distance between H440 N δ and E327 O ϵ increases from 2.52 Å in the native structure to 4.01 Å in the *TcAChE*–rivastigmine conjugate, while the distance between H440 N δ and E199 O ϵ decreases concomitantly from 3.49 to 2.85 Å. Moreover, the position of the main chain (C α) carbon atom of H440 in the *TcAChE*–rivastigmine structure moves by 0.64 Å relative to its position in the native enzyme structure.

3D Crystal Structure of the *TcAChE*–NAP Complex. The 3D structure of the complex of *TcAChE* with NAP alone

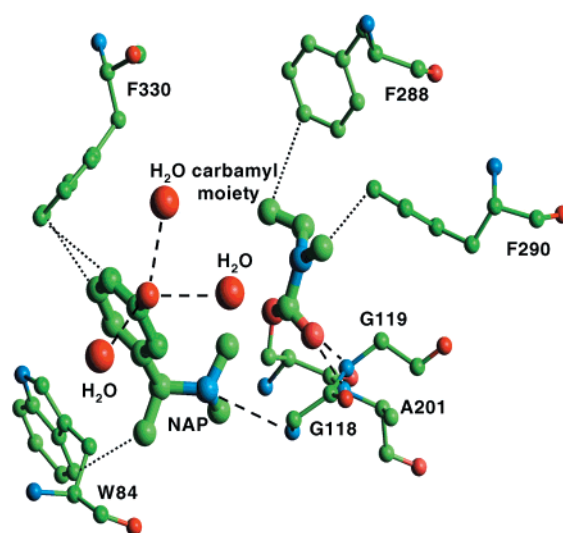


FIGURE 6: Active site of *TcAChE* after inhibition with rivastigmine. Amino acid residues within the active site of AChE that may interact with the inhibitor are shown. Rivastigmine is depicted with larger spheres and thicker lines for emphasis. The carbamyl portion of rivastigmine is positioned to make two H-bonds (dashed lines) with the amide nitrogens of A201 and G119, as well as nonbonded contacts (dotted lines) with F288 and F290 in the acyl pocket. NAP, the aromatic leaving group of rivastigmine, remains in the active site of crystalline AChE. NAP is within H-bonding distance of three water molecules (large red spheres), as well as of the amide nitrogen of G118. Nonbonding contacts and π – π interactions with W84 and F330 are depicted as dotted lines.

was determined, to find out whether the location and orientation of NAP in the complex are similar to those seen when NAP is generated in situ, concomitantly with carbamylation by rivastigmine. In Figure 8, NAP can be seen at approximately the same location as in the *TcAChE*–rivastigmine conjugate, but in a different orientation. The three water molecules near the NAP moiety are not seen, most likely due to the resolution being lower than in the rivastigmine conjugate. The aromatic–aromatic interactions of NAP with W84 and F330 are retained as in the *TcAChE*–rivastigmine structure. The NAP phenyl ring packs at an angle of $\sim 45^\circ$ to W84 with a distance between W84 C $\zeta 2$ and C7 of the NAP phenyl ring of 3.81 Å, and the ring of F330 is edge-on to the NAP phenyl ring, with a distance between F330 C $\epsilon 1$ and C9 of the NAP phenyl ring of 3.75 Å. The hydroxyl oxygen of NAP forms a 2.82 Å H-bond with E199 O ϵ , and the tertiary ammonium side chain is oriented toward the acyl binding pocket and the oxyanion hole. The orientations of W84 and of the residues in the oxyanion hole and in the acyl pocket, in both the rivastigmine conjugate and the NAP complex, are similar to their orientations in the native enzyme (Figure 7). The orientation of the F330 phenyl ring, which shows a high degree of variability in the various previously determined AChE–ligand complexes (13, 16), is quite different than in the *TcAChE*–rivastigmine conjugate, but similar to those of the huperzine A–, edrophonium–, and TMTFA–*TcAChE* complexes (16) (Figure 7). The position of the H440 imidazole ring in the *TcAChE*–NAP complex is very similar to its position in the native enzyme (Figure 7), with distances between H440 N δ and E327 O ϵ and between H440 N δ and E199 O ϵ of 2.67 and 3.29 Å, respectively. Thus, binding of

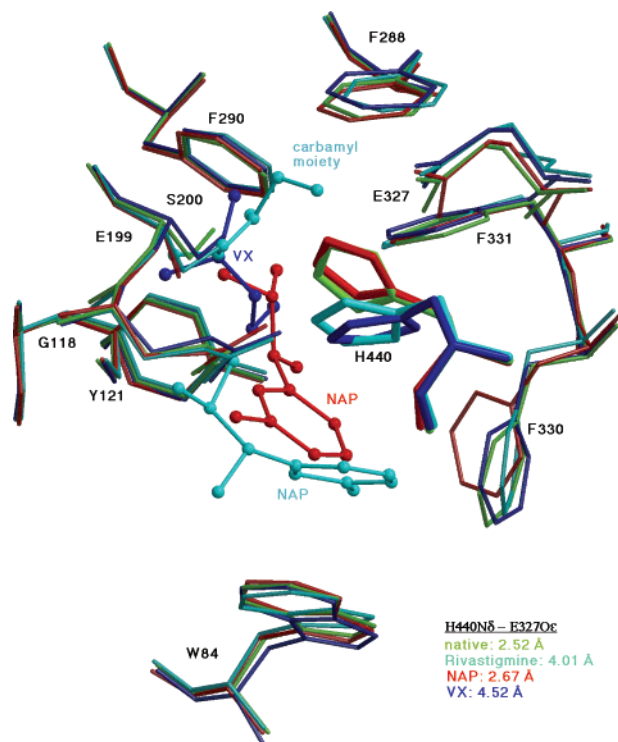


FIGURE 7: Comparison of the orientation of H440 in native *TcAChE*, the *TcAChE*–rivastigmine conjugate, the *TcAChE*–NAP complex, and the *TcAChE*–VX conjugate. An overlay of the active-site gorge in the four structures is presented. H440 is displayed using thicker lines for emphasis, and the inhibitors are shown as ball-and-stick models. Native *TcAChE* is colored green. The *TcAChE*–NAP complex is colored red. The *TcAChE*–rivastigmine conjugate is colored cyan. The *TcAChE*–VX conjugate is colored blue.

NAP produces no significant movement of the catalytic histidine.

DISCUSSION

The experimental data presented here provide novel kinetic and structural insights into the interaction of rivastigmine with *TcAChE*, in particular, and with ChEs, in general. First of all, we show that rivastigmine is a stereoselective, slow substrate of ChEs, not a simple reversible inhibitor. Second, rivastigmine shows a pronounced selectivity among various

types of ChEs because it reacts relatively poorly with *TcAChE*, whereas the carbamylation rate constants for other ChEs are rapid and more comparable with the rate reported for other carbamates. Finally, we find that decarbamylation (spontaneous reactivation) is unusually slow for all four ChEs that have been studied, with the carbamylated *TcAChE*–rivastigmine conjugate being the most refractory to reactivation.

The X-ray crystallography experiments fully support and clarify our kinetic findings. Rivastigmine reacts stoichiometrically (1:1) with S200 in the active site of *TcAChE* to form a stable ethylmethylcarbamylated enzyme (Figure 6). This directly supports the model of Wilson (39, 40), which treated carbamates as slow substrates of ChEs. The structural basis for the unusually low bimolecular rate constant for inhibition of the *Torpedo* enzyme is not immediately apparent. If the bulky leaving group of rivastigmine is replaced with a chloride moiety, the bimolecular rate constant is increased, but only 10-fold, which still makes it more than 2 orders of magnitude lower than that for inhibition of rhAChE. The structures of the *Torpedo* and human enzymes are very similar (47), and no dramatic difference can be distinguished in the dimensions of the acyl pocket. Replacement of F330 with a tyrosine residue (Y337 in rhAChE) produces a mutant in which the 14 aromatic residues lining the active site gorge are identical to the homologous residues in rhAChE. Y337 was shown to increase the rate constant for the inhibition of recombinant hAChE by huperzine A (48). Therefore, we modeled rivastigmine into F330Y *TcAChE* to see if this might help to explain the different rates of carbamylation of the two enzymes by rivastigmine. Figure 9 shows that the tyrosine residue is located between the carbamyl moiety and NAP, unlike F330 that is close to and makes interaction only with the NAP moiety in the *TcAChE*–rivastigmine conjugate. The hydroxyl group of Y330 can make four possible tight interactions. These are with the nitrogen of the carbamyl moiety (3.26 Å), with the ethyl group of the carbamyl moiety (3.0 Å), with the methyl group of the NAP moiety (3.17 Å), and with H440 N δ (2.87 Å). To place Y330 in the model, we had to change the positions of both H440 and F331, thus pushing H440 back toward E327 (3.0 Å compared to 4.0 Å), and away from E199 (3.65 Å compared to 2.85 Å), causing less disruption

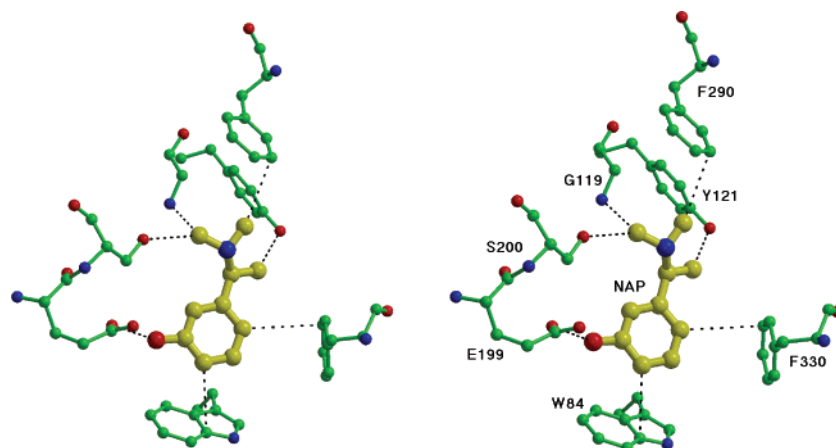


FIGURE 8: Stereoview of the active site of *TcAChE* complexed with NAP. NAP is depicted as a large ball-and-stick model for emphasis, with carbon atoms colored yellow, oxygen atoms colored red, and nitrogen atoms colored blue. Selected protein residues are rendered in ball-and-stick format, with carbon atoms colored green and labeled appropriately.

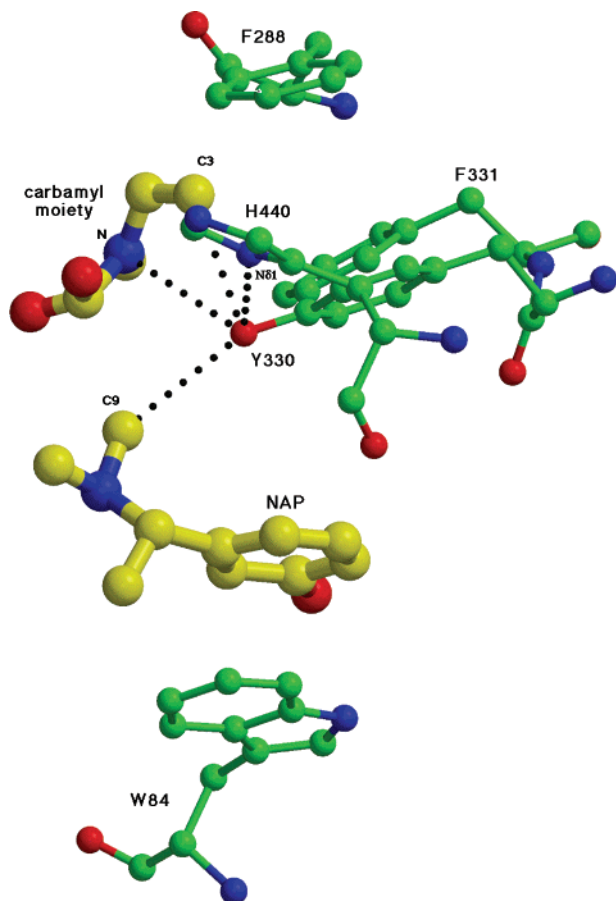


FIGURE 9: Model of the F330Y-*TcAChE*–rivastigmine conjugate. The carbamyl moiety and NAP are depicted as large ball-and-stick models for emphasis, with carbon atoms colored yellow, oxygen atoms colored red, and nitrogen atoms colored blue. Selected protein residues are depicted in ball-and-stick format, and colored green. The dotted lines are the four possible interactions made by Y330. The hydroxyl oxygen may form H-bonds with H440N (N δ 1), and with the amino nitrogen of the carbamyl moiety (N). Two other interactions are with the aminomethyl carbon of NAP (C9) and with the aminoethyl carbon of the carbamyl moiety (C3).

of the catalytic triad, which might result in both faster inhibition and reactivation.

The observed differences in the rates of inhibition of *TcAChE* and rhAChE by rivastigmine are reminiscent of the observations showing that phenylmethanesulfonyl fluoride (PMSF) does not inhibit electric organ AChE of either *Electrophorus* (49, 50) or *Torpedo* (51), although mammalian AChEs are inhibited well by PMSF, and *TcAChE* itself is inhibited well by benzenesulfonyl fluoride (51), which is smaller by only a methyl group. The differences in the susceptibility of the *Torpedo* and human enzymes to PMSF have been ascribed to a greater “breathing” capacity of the latter (51), and a similar explanation may hold for the differential susceptibility to rivastigmine.

The differences in the interaction of hBChE and *TcAChE* with rivastigmine can be rationalized as being due to differences between the two enzyme structures (52). BChE has a more open active site. Thus, movement of the histidine residue may not occur upon carbamylation of BChE, and if it is displaced, it may have more freedom to flip back. Thus, the more rapid inhibition and reactivation can both be rationalized. Recently, Kraut et al. (51) showed that the

double acyl pocket mutant of *TcAChE* (F288L/F290V), which converts the acyl pocket of AChE to that of BChE (52), produces susceptibility to inhibition by PMSF, to which the wild-type enzyme is completely resistant.

The 3D structure of r*DmAChE* (43) reveals that the active-site gorge of the insect enzyme is significantly narrower than that of *TcAChE*. In particular, the volume of the lower part of the gorge in the insect enzyme is ~50% of that in *TcAChE*. However, *DmAChE* has the ability to hydrolyze substrates with larger acyl moieties, such as butyrylcholine (53). Comparison of the *TcAChE* and r*DmAChE* structures shows that the catalytic triad, the residues forming the oxyanion hole, and the anionic binding site overlap well. However, a change in the shape of the acyl binding pocket results from differences in two important amino acid residues, F288 (L328 in r*DmAChE*) and V400 (F440 in r*DmAChE*). F288 and F331 in *TcAChE* form a rigid π – π stacking pair. The loss of the rigid stacking renders F371 (F331 in *TcAChE*) more mobile, thus enabling the insect binding pocket to accommodate larger moieties. Moreover, in the *TcAChE*–rivastigmine conjugate, the amino group of the carbamyl moiety, with its ethyl and methyl substituents, is oriented toward F288 in the acyl pocket (3.2 Å). When the coordinates of rivastigmine were inserted into the r*DmAChE* map (not shown), this interaction was lost. However, five new strong interactions between the ethyl group of the carbamyl moiety and F440 appeared to be formed. In addition, as in rhAChE, in r*DmAChE*, too, F330 is replaced with a tyrosine in the array of aromatics lining the acyl pocket, which might also affect the kinetics of inhibition and reactivation of r*DmAChE* with rivastigmine.

The extremely slow reactivation of the carbamylated enzyme is a feature shared by all four ChEs that have been examined. Thus, even though the *Torpedo* conjugate is the most refractory to reactivation, with an extrapolated half-life of >500 h at 25 °C, even for the other enzymes, half-lives in the range of 10^2 – 10^3 h can be estimated for reactivation at room temperature.

The crystallographic data support the hypothesis that, for *TcAChE*, slow reaction is due to a synergistic effect of the ethylmethylcarbamyl moiety and of the NAP leaving group, bound to the anionic site (though at less than full occupancy). Reaction with rivastigmine resulted in disruption of the catalytic triad, apparently due to NAP causing a movement of H440 away from E327. Alternatively, the movement of H440 might occur by NAP orienting the transition state such that the *N*-ethylmethyl group crowds the histidine. Due to steric exclusion, the new orientation of the active-site histidine does not permit the approach of a water molecule to the correct position of the carbamyl moiety for nucleophilic attack. The ethyl group on the nitrogen of the carbamyl moiety, which is a relatively bulky group, makes this even harder. The fact that there is no movement of the catalytic histidine in the *TcAChE*–NAP complex can be explained as being due to the absence of the carbamyl moiety, thus allowing NAP enough room to be accommodated in the anionic site without causing any conformational changes. *TcAChE* inhibited by EMCC undergoes reactivation at a rate comparable to those of other dialkylcarbamyl-ChE conjugates, as do the corresponding rhAChE and BChE conjugates. Furthermore, even if NAP is added to a preformed conjugate, reactivation is not substantially retarded. Thus, NAP either

cannot penetrate into the anionic site of carbamylated *TcAChE* or, if able to penetrate, cannot act synergistically with the carbamyl group to disrupt the catalytic triad as it does when generated in situ. The fact that for all four ChEs that have been examined, reactivation of the conjugate generated by rivastigmine is extremely slow favors the notion that the catalytic triad is similarly disrupted in all four.

Crystallographic data were recently presented showing that the nonaged conjugate produced by phosphorylating *TcAChE* with the potent nerve agent *O*-ethyl-*S*-{2-[bis(1-methylethyl)-amino]ethyl}methylphosphonothioate (VX) similarly displays a disrupted catalytic triad (54). Whether a synergistic effect of the leaving group is involved in this case, too, is not known. In any event, it is not retained in the crystal structure of the organophosphonyl-*TcAChE* conjugate. Comparison of the *TcAChE*–rivastigmine conjugate and the *TcAChE*–VX conjugate, both determined at 2.2 Å resolution, reveals that the catalytic histidine is mobile. H440 N δ moves away from its resting state partner, E327 O ϵ , in the *TcAChE*–rivastigmine conjugate and in the *TcAChE*–VX conjugate, by 4.01 and 4.52 Å, respectively, and is within H-bond range of E199 O ϵ at distances of 2.85 and 2.64 Å, respectively (Figure 7). After the *TcAChE*–VX conjugate has been aged, the catalytic triad is regenerated. Whether regeneration of the triad occurred concomitantly with aging, or was delayed, is not known, since aging occurred in the crystalline conjugate at 4 °C over a period of several weeks.

Bartolucci et al. (55) earlier published the structure of a complex of the physostigmine analogue, 8-(*cis*-2,6-dimethylmorpholino)octylcarbamoyloseroline (MF268), with *TcAChE*. As in the case of the *TcAChE*–rivastigmine conjugate, inhibition appears to be irreversible, with no significant reactivation occurring over a period of days (56). However, no significant conformational change was observed in comparison to the native enzyme, nor was the leaving group retained in the crystal structure. The carbamyl moiety contains a dimethylmorpholinooctyl chain, which stretches along the active-site gorge, and irreversibility was ascribed to the presence of this chain, with the bulky dimethylmorpholino group at the gorge entrance, limiting access of hydrolytic water molecules to the active site. The conjugate of another physostigmine analogue, eptastigmine, which is now in Phase III clinical trials (57), and bears a free octyl substituent on its carbamyl moiety, does reactivate, but with a very long half-life of 11 days (56).

Rivastigmine is a “pseudo-irreversible” inhibitor of AChE since decarbamylation is very slow (hours to days). Consequently, inhibition of AChE is expected to persist even after the drug has been cleared from the plasma. Tolerated doses of rivastigmine are 3–12 mg/day (58), and large clinical trials confirm that the agent produces clinically relevant improvements in cognitive function with minimal unwanted adverse effects on patients with mild to moderate AD (59, 60). The results presented in this report show a strong species dependence of the kinetic data for interaction of rivastigmine with AChE, necessitating caution in extrapolating from one species to another. Moreover, there are major differences between the results obtained in vivo and in vitro. The pharmacological profile of rivastigmine in vivo showed that it binds to BChE with a 10-fold lower affinity than to the G₁ form of AChE (27), and that it selectively inhibits AChE in the CSF relative to both peripheral AChE and BChE (61).

Our in vitro studies clearly show that rivastigmine is a more potent inhibitor of hBChE than of rhAChE. Possible differences in molecular structure (e.g., degrees of oligomerization and glycosylation) between CSF AChE and both the peripheral and recombinant enzymes may be responsible for these differences.

NAP, the leaving group of rivastigmine, is itself a competitive inhibitor (Figure 3). If NAP is administered orally to rats, no inhibition of brain AChE is detected, probably due to poor penetrability and rapid clearance (A. Enz, unpublished observations). However, it must certainly be generated at substantial levels in situ, concomitantly with carbamylation of brain AChE by rivastigmine. This might explain why maximum inhibition of rat brain AChE by rivastigmine was only 80–90% (A. Enz, unpublished observations), despite the almost irreversible action of the carbamate.

Our findings that rivastigmine is not a simple reversible inhibitor and that its leaving group, NAP, also inhibits AChE suggest that more detailed studies should be undertaken to establish the best kinetic models, both in vitro and in vivo, as well as the individual reaction rate constants for this important drug. Employment of suitable mutant enzymes should also help to resolve some of the open questions.

REFERENCES

1. Taylor, P. (1990) in *The Pharmacological Basis of Therapeutics* (Gilman, A. G., Nies, A. S., Rall, T. W., and Taylor, P., Eds.) 5th ed., pp 131–150, MacMillan, New York.
2. Quinn, D. M. (1987) *Chem. Rev.* 87, 955–975.
3. Sussman, J. L., Harel, M., Frolow, F., Oefner, C., Goldman, A., Toker, L., and Silman, I. (1991) *Science* 253, 872–879.
4. Bowen, D. M., Smith, C. B., White, P., and Davison, A. N. (1976) *Brain* 99, 459–496.
5. Davies, P. (1979) *Brain Res.* 171, 319–327.
6. Bartus, R. T., Dean, R. L. d., Beer, B., and Lippa, A. S. (1982) *Science* 217, 408–414.
7. Dunnett, S. B., and Fibiger, H. C. (1993) *Prog. Brain Res.* 98, 413–420.
8. Weinstock, M. (1997) *J. Neural Transm., Suppl.* 49, 93–102.
9. Giacobini, E. (2000) in *Cholinesterases and Cholinesterase Inhibitors* (Giacobini, E., Ed.) pp 181–226, Martin Dunitz, London.
10. Zhang, R. W., Tang, X. C., Han, Y. Y., Sang, G. W., Zhang, Y. D., Ma, Y. X., Zhang, C. L., and Yang, R. M. (1991) *Zhongguo Yaoli Xuebao* 12, 250–252.
11. Harvey, A. L. (1995) *Pharmacol. Ther.* 68, 113–128.
12. Greenblatt, H. M., Kryger, G., Lewis, T., Silman, I., and Sussman, J. L. (1999) *FEBS Lett.* 463, 321–326.
13. Harel, M., Schalk, I., Ehret-Sabatier, L., Bouet, F., Goeldner, M., Hirth, C., Axelsen, P. H., Silman, I., and Sussman, J. L. (1993) *Proc. Natl. Acad. Sci. U.S.A.* 90, 9031–9035.
14. Davis, K. L., and Powchik, P. (1995) *Lancet* 345, 625–630.
15. Kawakami, Y., Inoue, A., Kawai, T., Wakita, M., Sugimoto, H., and Hopfinger, A. J. (1996) *Bioorg. Med. Chem.* 4, 1429–1446.
16. Kryger, G., Silman, I., and Sussman, J. L. (1999) *Structure* 7, 297–307.
17. Hemsworth, B. A., and West, G. B. (1968) *J. Pharm. Pharmacol.* 20, 406–407.
18. Stedman, E., and Banger, G. (1925) *J. Chem. Soc.* 127, 247–258.
19. Koelle, G. B. (1963) in *Handbuch der Experimentellen Pharmakologie*, Springer-Verlag, Heidelberg, Germany.
20. Stedman, E. (1929) *Biochem. J.* 23, 17–24.
21. Stedman, E. (1929) *Am. J. Physiol.* 90, 528–529.

22. Stedman, E., and Stedman, E. (1931) *Biochem. J.* 25, 1147–1167.
23. Easson, L. H., and Stedman, E. (1933) *Biochem. J.* 27, 1257–1266.
24. Weinstock, M., Razin, M., Chorev, M., and Tashma, Z. (1986) in *Advances in Behavioral Biology* (Fisher, A., Hanin, I., and Lachman, C., Eds.) pp 539–551, Plenum Press, New York.
25. Weinstock, M., Razin, M., Ringel, I., Tashma, Z., and Chorev, M. (1992) in *Multidisciplinary Approaches to Cholinesterase Functions* (Shafferman, A., and Velan, B., Eds.) pp 251–259, Plenum Press, New York.
26. Thal, L. J., Fuld, P. A., Masur, D. M., and Sharpless, N. S. (1983) *Ann. Neurol.* 13, 491–496.
27. Enz, A., Boddeke, H., Gray, J., and Spiegel, R. (1991) *Ann. N.Y. Acad. Sci.* 640, 272–275.
28. Futerman, A. H., Low, M. G., and Silman, I. (1983) *Neurosci. Lett.* 40, 85–89.
29. Sussman, J. L., Harel, M., Frolow, F., Varon, L., Toker, L., Futerman, A. H., and Silman, I. (1988) *J. Mol. Biol.* 203, 821–823.
30. Raves, M. L., Harel, M., Pang, Y. P., Kozikowski, A. P., and Sussman, J. L. (1997) *Nat. Struct. Biol.* 4, 57–63.
31. Grunwald, J., Marcus, D., Papier, Y., Raveh, L., Pittel, Z., and Ashani, Y. (1997) *J. Biochem. Biophys. Methods* 34, 123–135.
32. Mallender, W. D., Szegletes, T., and Rosenberry, T. L. (1999) *J. Biol. Chem.* 274, 8491–8499.
33. Incardona, J. P., and Rosenberry, T. L. (1996) *Mol. Biol. Cell* 7, 595–611.
34. Ellman, G. L., Courtney, K. D., Anders, V., and Featherstone, R. M. (1961) *Biochem. Pharmacol.* 7, 88–95.
35. Cornish-Bowden, A. (1976) in *Principles in Enzyme Kinetics*, pp 52–70, Butterworths, London.
36. Penefsky, H. S. (1979) *Methods Enzymol.* 56, 527–530.
37. Adams, P. D., Pannu, N. S., Read, R. J., and Brunger, A. T. (1997) *Proc. Natl. Acad. Sci. U.S.A.* 94, 5018–5023.
38. Brunger, A. T., Adams, P. D., Clore, G. M., DeLano, W. L., Gros, P., Grosse-Kunstleve, R. W., Jiang, J. S., Kuszewski, J., Nilges, M., Pannu, N. S., Read, R. J., Rice, L. M., Simonson, T., and Warren, G. L. (1998) *Acta Crystallogr. D54*, 905–921.
39. Wilson, I. B., Hatch, M. A., and Ginsburg, S. (1960) *J. Biol. Chem.* 235, 2312–2315.
40. Wilson, I. B., Harrison, M. A., and Ginsburg, S. (1961) *J. Biol. Chem.* 236, 1498–1500.
41. Aldridge, W. N., and Reiner, E. (1972) in *Enzyme Inhibitors as Substrates: Interactions of Esterases with Esters of Organophosphorus and Carbamic Acids*, pp 123–145, North-Holland Publishing Co., Amsterdam.
42. Kreimer, D. I., Dolginova, E. A., Raves, M., Sussman, J. L., Silman, I., and Weiner, L. (1994) *Biochemistry* 33, 14407–14418.
43. Harel, M., Kryger, G., Rosenberry, T. L., Mallender, T. L., Fletcher, R. J., Guss, M., Silman, I., and Sussman, J. L. (2000) *Protein Sci.* 9, 1–10.
44. Kreimer, D. I., Shnyrov, V. L., Villar, E., Silman, I., and Weiner, L. (1995) *Protein Sci.* 4, 2349–2357.
45. Harel, M., Quinn, D. M., Nair, H. K., Silman, I., and Sussman, J. L. (1996) *J. Am. Chem. Soc.* 118, 2340–2346.
46. Koellner, G., Kryger, G., Millard, C. B., Silman, I., Sussman, J. L., and Steiner, T. (2000) *J. Mol. Biol.* 296, 713–735.
47. Kryger, G., Harel, M., Giles, K., Toker, L., Velan, B., Lazar, A., Kronman, C., Barak, D., Ariel, N., Shafferman, A., Silman, I., and Sussman, J. L. (2000) *Acta Crystallogr. D56*, 1385–1394.
48. Ashani, Y., Grunwald, J., Kronman, C., Velan, B., and Shafferman, A. (1994) *Mol. Pharmacol.* 45, 555–560.
49. Gold, A. M., and Fahrney, D. (1966) *Biochemistry* 5, 2911–2913.
50. Moss, D. E., and Fahrney, D. (1978) *Biochem. Pharmacol.* 27, 2693–2698.
51. Kraut, D., Goff, H., Pai, R. K., Hosea, N. A., Silman, I., Sussman, J. L., Taylor, P., and Voet, J. G. (2000) *Mol. Pharmacol.* 57, 1243–1248.
52. Harel, M., Sussman, J. L., Krejci, E., Bon, S., Chanal, P., Massoulié, J., and Silman, I. (1992) *Proc. Natl. Acad. Sci. U.S.A.* 89, 10827–10831.
53. Gnagey, A. L., Forte, M., and Rosenberry, T. L. (1987) *J. Biol. Chem.* 262, 13290–13298.
54. Millard, C. B., Koellner, G., Ordentlich, A., Shafferman, A., Silman, I., and Sussman, J. L. (1999) *J. Am. Chem. Soc.* 121, 9883–9884.
55. Bartolucci, C., Perola, E., Cellai, L., Brufani, M., and Lamba, D. (1999) *Biochemistry* 38, 5714–5719.
56. Perola, E., Cellai, L., Lamba, D., Filocamo, L., and Brufani, M. (1997) *Biochim. Biophys. Acta* 1343, 41–50.
57. Imbimbo, B. P., Troetel, W. M., Martelli, P., and Lucchelli, F. (2000) *Dementia Geriatr. Cognit. Disord.* 11, 17–24.
58. Sramek, J. J., Anand, R., Wardle, T. S., Irwin, P., Hartman, R. D., and Culter, N. R. (1996) *Life Sci.* 58, 1201–1207.
59. Corey-Bloom, J., Anand, R., and Veach, J. (1998) *Int. J. Geriatr.* 1, 55–65.
60. Rosler, M., Anand, R., Cicin-Sain, A., Gautier, S., Agid, Y., Dal-Bianco, P., Stahelin, H. B., Hartman, R., Gharabawi, M., and Group, B. E. S. (1999) *BMJ* 318, 633–638.
61. Kennedy, J. S., Polinsky, R. J., Johnson, B., Loosen, P., Enz, A., Laplanche, R., Schmidt, D., Mancione, L. C., Winston, C. V., and Ebert, M. H. (2000) *J. Clin. Psychopharm.* 19, 513–521.

BI020016X